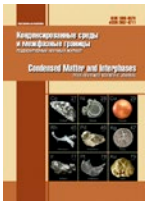

ISSN 1606-867X (Print)
ISSN 2687-0711 (Online)
Condensed Matter and Interphases
Kondensirovannye Sredy i Mezhfaznye Granitsy
https://journals.vsu.ru/kcmf/

Original articles

Research article
https://doi.org/10.17308/kcmf.2024.26/12447

The effect of the aging time of the $ZrO_2 \cdot nH_2O$ coagel: features of its phase formation and the evolution of its adsorption properties

Sh. O. Omarov[1]✉, N. A. Pakhomov[2]

[1]Ioffe Institute,
26 ul. Politechnicheskaya, Saint Petersbutg 194021, Russian Federation

[2]St. Petersburg State Technological Institute (Technical University),
26 Moskovskiy pr., Saint Petersbutg 190013, Russian Federation

Abstract

To date, researchers have failed to provide a physicochemical explanation of the crystallization of low-soluble X-ray amorphous $ZrO_2 \cdot nH_2O$ caused by its aging in contact with the mother liquor. Data obtained in previous studies may be erroneous due to the unpredictable effect of Si^{4+}, Na^+ and K^+ impurity ions. This study is aimed at establishing the regularities and features of the phase formation, as well as changes in the adsorption properties of $ZrO_2 \cdot nH_2O$ and the functional composition of the ZrO_2 surface depending on the aging time of the $ZrO_2 \cdot nH_2O$ coagel in contact with the mother solution and in absence of impurity ions. The research was carried out on $ZrO_2 \cdot nH_2O$ obtained by direct precipitation at pH = 10 followed by aging for 6–406 h in a fluoroplastic reactor and on ZrO_2 obtained by heat treatment of the corresponding $ZrO_2 \cdot nH_2O$ at 500 °C.

The properties of $ZrO_2 \cdot nH_2O$ and ZrO_2 were studied by methods of synchronous thermal analysis, X-ray diffraction, scanning electron microscopy, low-temperature N_2 sorption, vacuum infrared spectroscopy, infrared spectroscopy, and temperature programmed desorption of molecular probes. It was shown that there is an extremum of the phase composition and adsorption properties of $ZrO_2 \cdot nH_2O$ and ZrO_2 after 24–96 h of aging.

It was established for the first time that the process of decomposition of dense aggregates of primary particles and submicron and micron aggregates and agglomerates of X-ray amorphous $ZrO_2 \cdot nH_2O$ accompanied by the appearance of edge OH-groups precedes its crystallization in contact with the mother solution (6–48 h). Further aging (96–406 h) revealed a gradual crystallization of $ZrO_2 \cdot nH_2O$ in the form of a mixture of the tetragonal and monoclinic phases of ZrO_2 in a 1:1 ratio as a result of the attachment of primary particles of $ZrO_2 \cdot nH_2O$ with the participation of edge and bridging OH groups. Acid-base properties of the ZrO_2 surface are in extreme dependence on the aging time. With prolonged aging (more than 213 hours), the acid function of the ZrO_2 surface begins to prevail due to the participation of the basic edge OH groups in the attachment of the $ZrO_2 \cdot nH_2O$ primary particles. The observed changes are discussed from the perspective of the theory of oriented attachment of nanocrystals.

Keywords: Zirconium, Dioxide, Hydrated, Phase, Porosity, Morphology, Attachment, Surface, Acidity, Basicity

Funding: The study was supported by the Ministry of Science and Higher Education of the Russian Federation within the framework of state order to Ioffe Institute of the Russian Academy of Sciences, project No. FFUG-2024-0036

Acknowledgments: The authors thank Tenevich M. I. for the study using the scanning electron microscopy method on the equipment of the Engineering Center of St. Petersburg State Technological Institute, as well as Fedorov S. P. and Serazhim M. S. for the study using the low-temperature nitrogen sorption method on the equipment of the Laboratory of Catalytic Technologies of St. Petersburg State Technological Institute.

For citation: Omarov Sh. O., Pakhomov N. A. The effect of the aging time of the $ZrO_2 \cdot nH_2O$ coagel: features of its phase formation and the evolution of its adsorption properties. *Condensed Matter and Interphases*. 2024;26(4): 732–744. https://doi.org/10.17308/kcmf.2024.26/12447

✉ Shamil O. Omarov, e-mail: somarov@mail.ioffe.ru

Для цитирования: Омаров Ш. О., Пахомов Н. А. Влияние длительности старения коагеля $ZrO_2 \cdot nH_2O$: особенности фазообразования и эволюции адсорбционных свойств. *Конденсированные среды и межфазные границы*. 2024;26(4): 732–744. https://doi.org/10.17308/kcmf.2024.26/12447

1. Introduction

Zirconium dioxide has been widely used in industry as the main component of ceramic, refractory, composite, and other materials [1]. The constant need in new catalysts with improved or unique properties explains increased attention to zirconium dioxide as a promising material for the production of domestic catalysts for refining and petrochemistry, the importance of which has increased in the context of import substitution [2].

The main obstacle to a wider use of ZrO_2 in this field is the difficulty of regulating its phase composition, poorly developed porosity, and acid-base surface properties. These characteristics can be improved either by changing the synthesis method and conditions [3, 4] in order to change the texture or by controlled introduction of promoters to stabilize the phase composition and adjust the surface properties. In the case of zirconium dioxide, the most popular has been the method of aging the hydrated precursor of $ZrO_2 \cdot nH_2O$ in contact with the mother solution under mild conditions ($T \leqslant 100$ °C, atmospheric pressure) [5–14]. The following synthesis parameters have been studied: aging time and temperature, suspension pH, the type of precipitant, the method of precipitation, etc. However, these studies share one disadvantage, they do not consider or control the effect of impurities on the phase formation, texture, and adsorption properties of ZrO_2. They are also characterised by insufficient aging time and fragmentary information about the crystallization of $ZrO_2 \cdot nH_2O$ in contact with the mother solution. Impurities can originate from alkaline precipitants (NaOH, KOH), and leached silicon from the reactor in an alkaline environment. Their effect is enhanced as they are accumulated during a prolonged aging. This problem can be solved by eliminating the factors that cause the presence of impurities, i.e. precipitation with an ammonia solution followed by the $ZrO_2 \cdot nH_2O$ aging in a reactor made from a chemically inert material. The study of the phase composition is complicated by the fact that zirconium dioxide can normally exist in two metastable modifications: a tetragonal *t*-ZrO_2 (space group $P4_2/nmc$) or cubic *c*-ZrO_2 (space group $Fm\text{-}3m$) [15, 16]. They are formed under the influence of various factors (size effect, oxygen vacancies, anionic and cationic impurities, OH-groups), which are also inherent in the modification which is thermodynamically stable monoclinic modification (space group $P2_1/c$) in normal conditions [14–17].

The influence of the conditions of the $ZrO_2 \cdot nH_2O$ aging on the changes in the porosity and phase composition of $ZrO_2 \cdot nH_2O$ and ZrO_2 can be explained, in particular, by repeated dissolution and repeated precipitation [6, 7, 9, 10]. These processes take place at pH = 13.7, at which crystallization of $ZrO_2 \cdot nH_2O$ to *t*-ZrO_2 was observed in [6] within 24 hours. However, the low solubility product of $ZrO_2 \cdot nH_2O$ ($K_{sp} = 10^{-57}–10^{-62}$) in a wide range of pHs [18, 19], nanoparticle sizes [20], and temperatures [21] does not allow considering repeated dissolution as the main cause of changes in the porosity and crystallization of $ZrO_2 \cdot nH_2O$ under the most common conditions of aging: pH = 4–10 and $T \leqslant 100$ °C. As a result, it is necessary to study alternative approaches to explaining the processes occurring during the aging of $ZrO_2 \cdot nH_2O$ and the phase formation of ZrO_2. One such approach is the oriented attachment theory (OAT) [22–26], the concepts of which have been used to explain the formation of anisotropic ZrO_2 particles with complex morphology under hydrothermal conditions [27–34].

The dependence of the acid-base properties of the ZrO_2 surface on the aging time of $ZrO_2 \cdot nH_2O$ remains unclear. The little available data [35] do not take into account the above-mentioned effect of impurities, which can unpredictably affect the adsorption properties of ZrO_2. This problem might be solved by using a set of methods to study the surface. In particular, temperature programmed desorption (TPD) of molecular probes is used to determine integral indicators of acidity and basicity. IR spectroscopy of adsorbed molecular probes allows qualitatively and quantitatively determining the type of Brønsted acid sites and Lewis acid sites.

The purpose of this study is to establish the regularities and features of the phase formation, as well as the changes in the adsorption properties of $ZrO_2 \cdot nH_2O$ and the functional composition of the ZrO_2 surface depending on the aging time of the $ZrO_2 \cdot nH_2O$ coagel in contact with the mother solution and in the absence of Si^{4+}, Na^+, and K^+ impurity ions. For this, the aging of $ZrO_2 \cdot nH_2O$ precipitated with ammonia solution was carried out in a polychlorotrifluoroethylene (PTFE) reactor for 406 hours, which was twice the time used in all previous studies carried out in this area. A set of methods was chosen to study the adsorption properties, i.e. low-temperature N_2 sorption, TPD, and IR spectroscopy of molecular probes, which allow for a comprehensive study of various aspects of the surface formation, as well as the changes in the texture of X-ray amorphous $ZrO_2 \cdot nH_2O$.

2. Experimental

$ZrO_2 \cdot nH_2O$ was synthesized by direct precipitation from a 0.62 M solution of $ZrOCl_2$ (ρ = 1.096 g/cm^3 at 20 °C) with a 13M ammonia solution (ρ = 0.913 g/cm^3 at 20 °C) in a 0.5 L glass beaker at 20 °C and pH = 10.0 ± 0.1. The flow rate of the ammonia solution was 0.7 ml/min, the draining time was 20 min. The rotation speed of the stirring shaft was within 400–500 rpm. Further continuous aging of $ZrO_2 \cdot nH_2O$ was carried out in a 500 mL PTFE beaker at 90±1 °C for 6, 24, 48, 96, 213, 334, and 406 h. NH_3 solution was added regularly to maintain the suspension pH within 9.9–10.1 (measured at (20±2) °C). The precipitate was washed off Cl^- and NH_4^+ with distilled water at the rate of 0.2–0.25 L of H_2O per 1 g (control of 0.1 n with an $AgNO_3$ solution). After washing, the precipitate was dried at 70 °C for 4 h and at 90 °C for 1 h. The heat treatment of $ZrO_2 \cdot nH_2O$ was carried out in a muffle furnace in a stepwise mode: 170 °C – 0.5 h; 250 °C – 0.5 h; 350 °C – 0.5 h; 430 °C – 0.5 h; 500 °C – 2 h (the rate of temperature increase was 4 °/min), followed by cooling in the furnace.

Weight loss, the temperature limits of the main thermal transformations, and the values of thermal effects were determined on a DTG-60A synchronous thermal analyzer (Shimadzu, Japan). The samples (15–20 mg) were heated at 10 °C/min to 800 °C in static air.

The phase composition was determined on an XRD–6100 diffractometer (Shimadzu, Japan) with a Cu anode, Ni filter, with slits D:S:R = 0.5°: 0.5°:0.15 mm. The imaging was performed at 0.02° interval and the exposure time at each point of 1.2 or 3 s. To calculate the volume content of t-ZrO_2 V_t (vol %), we used the technique described in [36]. The Selyakov-Scherrer formula (K = 0.94; $\lambda(CuK\alpha_1)$ = 0.15406 nm) was used to calculate the coherent scattering regions (CSR) of the t-ZrO_2 (d_t, nm) and m-ZrO_2 (d_m, nm) phases.

The amount of the amorphous phase in the non-thermal treated samples was determined by absolute background calibration at 26° (2θ). For calibration, we used mixtures (10% : 90%, 50% : 50%, and 90% : 10% wt. ZrO_2) of the initial non-aged $ZrO_2 \cdot nH_2O$; t-ZrO_2, which had been obtained by heat treatment of the specified $ZrO_2 \cdot nH_2O$ at 500 °C; and reactive m-ZrO_2 with CSR = 20–25 nm.

The morphology of $ZrO_2 \cdot nH_2O$ powder particles was studied on a VEGA 3 SBH scanning electron microscope (Tescan, Czech Republic) in the backscattered electron mode.

The texture characteristics were studied by the method of low-temperature N_2 sorption on an Autosorb 6iSA unit (Quantachrome, USA) at –196 °C. The samples (0.04–0.2 g) were degassed under vacuum at 100 °C (for $ZrO_2 \cdot nH_2O$) or 250 °C (for the heat-treated samples) for 1 h. The value of the specific surface area (SSA, m^2/g) was calculated by the multipoint BET method; the total pore volume (V_Σ, cm^3/g) was calculated by the limit value of absorbed N_2 at p/p_0 = 0.99; the average pore size (d_{pore}, nm) relative to $4V_\Sigma/SSA$ and the pore size distribution were calculated by the density functional method using a nucleus for slit pores (QSDFT, equilibrium mode) for $ZrO_2 \cdot nH_2O$ or cylindrical pores (NLDFT, adsorption branch) for ZrO_2.

The hydroxyl cover of $ZrO_2 \cdot nH_2O$ was studied on an IrTracer-100 IR-Fourier spectrometer (Shimadzu, Japan) with an HTC-3-S12 vacuum attachment (Harrick, USA). For this, 10–15 mg of powder was compressed at a pressure of 1–2 t into a tablet with a diameter of 13 mm. Then, the tablet was placed in a cuvette, heated in a vacuum to 350 °C at a rate of 10° C/min, and kept for 10 minutes. After that, the IR spectrum of the sample was taken.

To study the acid-base properties of the ZrO_2 surface by IR spectroscopy of molecular probes, 15–25 mg of the ground catalyst sample was

compressed at a pressure of 3–4 t into a tablet with a diameter of 13 mm. The cuvette with the tablet was heated in vacuum to 360 °C and kept for 20 min. The time of the pyridine or CO_2 adsorption was 20 min after the cuvette cooled down to 150 °C. Spectra of the sorbed pyridine or CO_2 were taken at 150, 250, and 350 °C after exposure at each of the temperatures for 20 minutes. The concentration of the sorbed pyridine at BAS and LAS was calculated according to [37].

The total acidity and basicity of the surface and the distribution of the centers by the adsorption strength were determined by the method of temperature programmed desorption of NH_3 and CO_2 on a Khemosorb chemisorption analyzer (*SOLO*, Russia). The thermal desorption products were analyzed using an MC7-200D quadrupole mass spectrometer (Institute for Analytical Instrumentation of the Russian Academy of Sciences). The sample was heated in the He flow (99.9995% vol.) to 500 °C at a rate of 20 °C/min, kept for 20–30 min, and then cooled to 110 °C/min. A mixture of 10% NH_3 or CO_2 in He (20 mL/min) was then passed, followed by pure carrier gas (20 mL/min) until the mass spectrometer signal stabilized at m/z = 16 or m/z = 44. Desorption curves were recorded when the sample was heated in He (20 ml/min) at a rate of 10 °C/min. The calibration of the mass spectrometer by the selected mass numbers was carried out using gas mixtures with a known concentration of NH_3 or CO_2 with a total flow rate at the outlet of the chemisorption analyzer of 20 ml/min.

3. Results and discussion

3.1. Characteristics of $ZrO_2 \cdot nH_2O$

The morphology of freshly precipitated $ZrO_2 \cdot nH_2O$ was represented mainly by arbitrary-shaped dense agglomerates with a size of 10–100 μm consisting of plate-like agglomerates of a smaller size (Fig. 1A). Aging at 90 °C/min for 6 h led to partial destruction of agglomerates, the appearance of cracks of about 2 μm in size, and a decrease in the bulk density of the powder from 1.2 to 0.6 g/ml (Fig. 1B). The plates that made up loose agglomerates became more distinguishable, and their sizes reached 20–40 μm with a thickness of 2 μm (Fig. 1B). A further increase in the aging time to 48 hours resulted in a deeper decomposition of loose agglomerates to spheroid aggregates of about 100–300 nm (Fig. 1C, D). The latter became compacted again after 334 h of aging (Fig. 1E, F).

The described change in the morphology was also accompanied by a significant restructuring of the $ZrO_2 \cdot nH_2O$ porosity. According to the N_2 sorption data, the initial $ZrO_2 \cdot nH_2O$ (0 h of aging) was characterized by a type Ib isotherm, which corresponded to the microporous structure (Fig. 2A) with a small number of small mesopores of 2–4 nm (Fig. 2B). $ZrO_2 \cdot nH_2O$, which had been

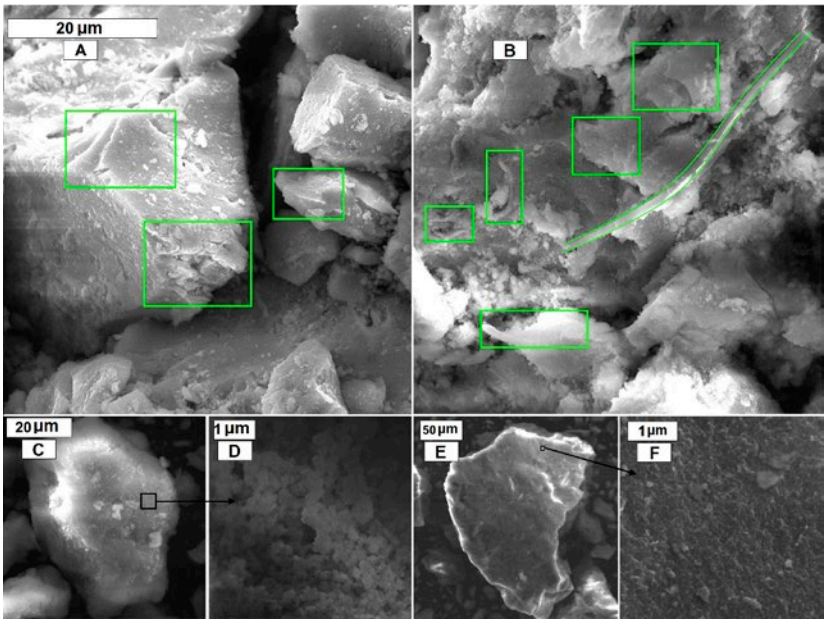

Fig. 1. SEM images of the $ZrO_2 \cdot nH_2O$ non-aged and aged under the mother liquor for 6 h (A, B), 48 h (C, D), and 334 h (E, F)

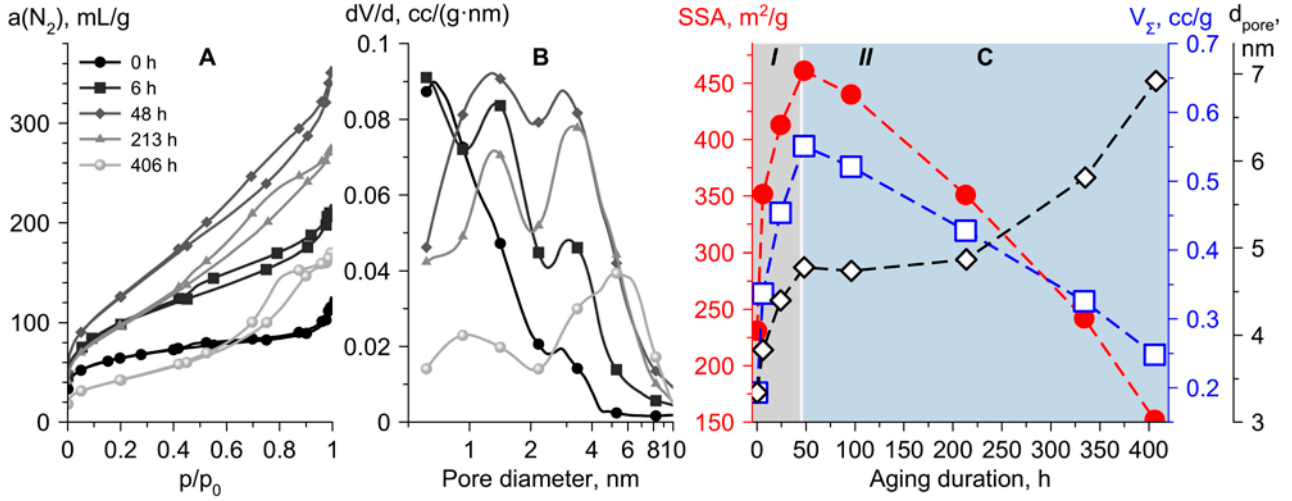

Fig. 2. Isotherms of N_2 sorption (A), pore size distribution (B), and dependence of textural characteristics (C) of $ZrO_2 \cdot nH_2O$ on the aging duration

aged for 6–48 hours, had an increased N_2 sorption at $p/p_0 > 0.4$ due to an increase in the contribution of a type IVA isotherm. This was also confirmed by an increase in the size of micropores from that close to ultramicropores to supermicropores of 1–2 nm and by the appearance of mesopores of 2–10 nm. The shape of the hysteresis loop changed from H4 (0 h) to H3 (6–48 h). Such changes indicate the decomposition of the initial dense microporous $ZrO_2 \cdot nH_2O$ aggregates to non-rigid aggregates of plate-like particles of the micro-mesoporous $ZrO_2 \cdot nH_2O$. Integral indicators of porosity (*SSA* and V_Σ) increased and reached their maximum (461 m^2/g and 0.55 cm^3/g) at 48 h.

Further aging for 96–406 h led to a decrease in the contribution of a type I isotrem and, accordingly, micropores, and a general decrease in the porosity indicators (*SSA* and V_Σ). The hysteresis loop of the 96 h sample corresponded to the H5 type (formation of open and partially closed mesopores), and of the 213–406 h samples to the H2a type (blind mesopores with narrow mouths), which was most distinct in the 406 h sample.

The results of the synchronous thermal analysis of $ZrO_2 \cdot nH_2O$ are shown in Fig. 3. The initial thermograms had several regions corresponding to the successive transformations of $ZrO_2 \cdot nH_2O$: stepwise dehydration at 30–125 and 125–300 °C, which resulted in the formation of a-ZrO_2 and were accompanied by removal of physically adsorbed water and a hydrated surface cover in the form of bridging and terminal OH groups (thermal decomposition of hydroxyoxide); and crystallization of a-ZrO_2 at 370–520 °C. An

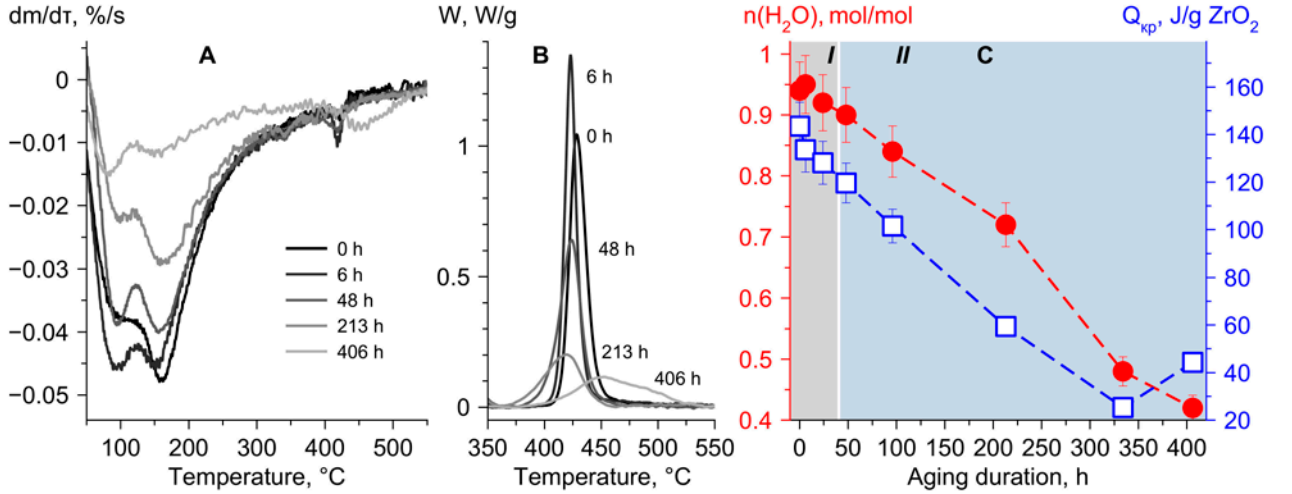

Fig. 3. DTG curves of $ZrO_2 \cdot nH_2O$ (A), the region of DTG curves of crystallization of a-ZrO_2 (B) and the dependence of hydration and crystallization heat of a-ZrO_2 (C) on the aging duration of $ZrO_2 \cdot nH_2O$

increase in the aging time to 48 h led to a slight decrease in the hydration of $ZrO_2 \cdot nH_2O$ and Q_{cr}, while further aging up to 406 h led to the deep dehydration and crystallization of $ZrO_2 \cdot nH_2O$. The dehydration of $ZrO_2 \cdot nH_2O$ during aging manifested itself mainly by a decrease in weight loss at the second stage of 125–300 °C.

X-ray phase analysis provided more information about the crystallization of $ZrO_2 \cdot nH_2O$ (Fig. 4). The X-ray amorphous state of the initial $ZrO_2 \cdot nH_2O$ (halo in the range of 20–40° 2θ) was maintained up to 48 h. The corresponding diffraction pattern had a slight increase in the intensity of approximately 30° 2θ. At 96 h, there were visible reflexes of t-ZrO_2 (111) and m-ZrO_2 (-111) (insert in Fig. 4A). Further aging resulted in the gradual crystallization of $ZrO_2 \cdot nH_2O$ and the formation of a mixture of t- and m-ZrO_2 and a phase ratio close to 1:1 (Fig. 4B). By 406 hours, the residual amount of a-ZrO_2 was 18% wt. The size of the t-ZrO_2 crystallites (CSR) was smaller than that of m-ZrO_2, but both tended to increase in size from 7.7 to 10.3 nm and from 14 to 18.1 nm, respectively (Fig. 4B).

3.2. Characteristics of ZrO_2

Heat treatment at 430 and 500 °C of freshly precipitated $ZrO_2 \cdot nH_2O$ led to the crystallization of the t-ZrO_2 phase (Fig. 5A) and the formation of large crystallites of 22–25 nm (Fig. 5B). As a

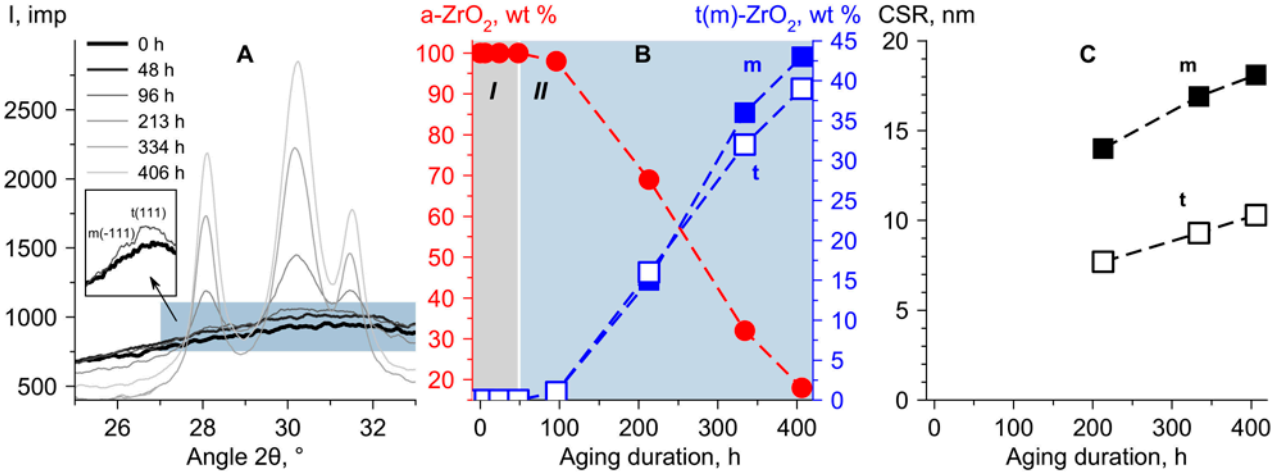

Fig. 4. Diffractograms of $ZrO_2 \cdot nH_2O$ (A), the dependence of the phase composition (B) and the CSR size of ZrO_2 phases (C) on the aging duration of $ZrO_2 \cdot nH_2O$

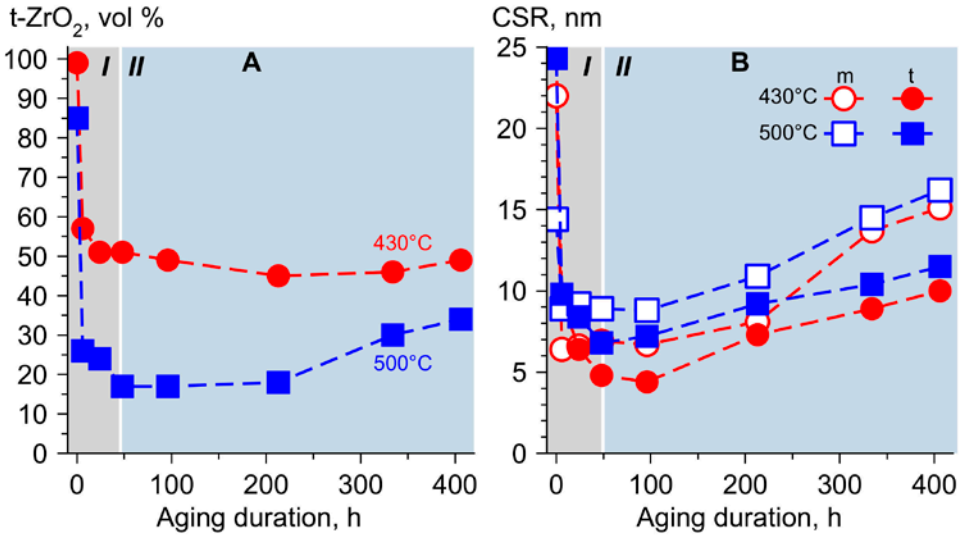

Fig. 5. The dependence of the phase composition (A) and the CSR size of ZrO_2 phases (430 and 500 °C) on the aging duration of $ZrO_2 \cdot nH_2O$ (B)

result of the $ZrO_2 \cdot nH_2O$ aging for 6 h, the *m*-ZrO_2 phase content increased significantly to 43% and the size of the crystallites decreased to 6 (10) nm at 430 °C (500 °C). With increasing aging time, the phase ratio remained close to 1 (430 °C). The minimum size of phase crystallites was achieved at 48–96 h of aging. Aging for 213–406 h led to a slight increase in the amount of *t*-ZrO_2 and an increase in the size of the CSR of the phases. The latter was in line with the trend in Fig. 4B and the size of ZrO_2 (430 °C) crystallites did not differ from the CSR of the phases for the corresponding $ZrO_2 \cdot nH_2O$.

The isotherms of N_2 sorption of all ZrO_2 samples after heat treatment at 500 °C (Fig. 6A) corresponded to type IVA, which was confirmed by the corresponding pore size distribution (Fig. 6B). The type of hysteresis loops varied: H3 (non-rigid aggregates of plate-like particles) for the ZrO_2 sample, whose $ZrO_2 \cdot nH_2O$ had not undergone aging; 6 h – H5; 24–213 (96) h – H2a (blind mesopores with narrow mouths) with signs of H3 or H5 (partially blocked ordered mesopores); 406 h – H1 (materials with blind pores with a close distribution over the width of the pore mouth and cavity or a narrow range of uniform open mesopores). The latter was further confirmed by a narrow pore size distribution (5.5–20.5 nm for 213 h and 7.3–24.6 nm for 406 h) (Fig. 6B).

The dependences of the porosity indicators, *SSA*, V_Σ, and d_{por}, of ZrO_2 on the aging time of the corresponding $ZrO_2 \cdot nH_2O$ were similar to those in Fig. 4. The maximum *SSA* (91 m^2/g) and V_Σ (0.32 cm^3/g) were achieved during aging for 48 h and heat treatment at 500 °C.

Since $ZrO_2 \cdot nH_2O$ has several types of OH groups (terminal, single- and triple-bridging, hydrogen bond between OH groups) [38–41], IR spectroscopy was used to study the change in the ratio between them depending on the aging time when $ZrO_2 \cdot nH_2O$ was heated to 350 °C in vacuum (Fig. 7). The absorption band corresponding to the terminal (edge) OH groups with a maximum of 3,760±5 cm^{-1} overlapped with the absorption band of the double-bridging OH groups with a maximum of 3,735±5 cm^{-1}. With an increase in the aging time, there was an extreme dependence of the ratio of the area of the terminal band to the sum of the areas of all bridging OH groups with a maximum at 48 hours of aging.

3.3. Acid-base properties of the ZrO_2 surface

Aging of $ZrO_2 \cdot nH_2O$ affects the acid-base properties of the surface of calcined ZrO_2 (500 °C). According to the data of TPD-NH_3 and TPD-CO_2 (Fig. 8), an increase in the aging time to 6–24 hours led to an increase in the specific acidity and basicity of the surface (Fig. 8A), especially of the basic sites. This result was apparently associated with the decomposition of the aggregates. On the one hand, it led to the appearance of Zr edge atoms dehydrated during heat treatment accompanied by the formation of LAS. On the other hand, the decomposition of aggregates contributed to an increase in the share of terminal OH groups (Fig. 7B), which had

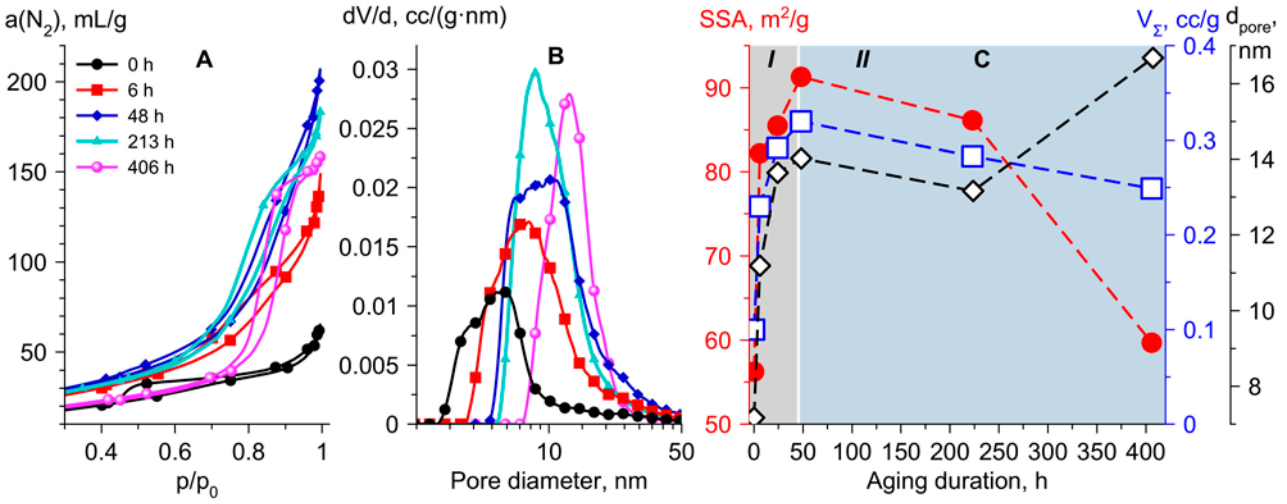

Fig. 6. Isotherms of N_2 sorption (A), pore size distribution, and dependence of textural characteristics (B) of ZrO_2 (500 °C) on the aging duration of $ZrO_2 \cdot nH_2O$

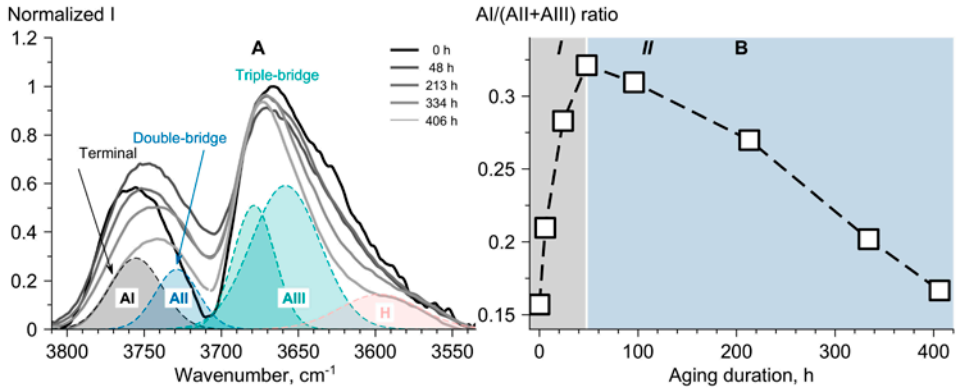

Fig. 7. IR spectra of $ZrO_2 \cdot nH_2O$ OH groups (A) and the dependence of the ratio of the absorption band area of terminal OH-groups and bridge OH-groups on the aging duration of (B)

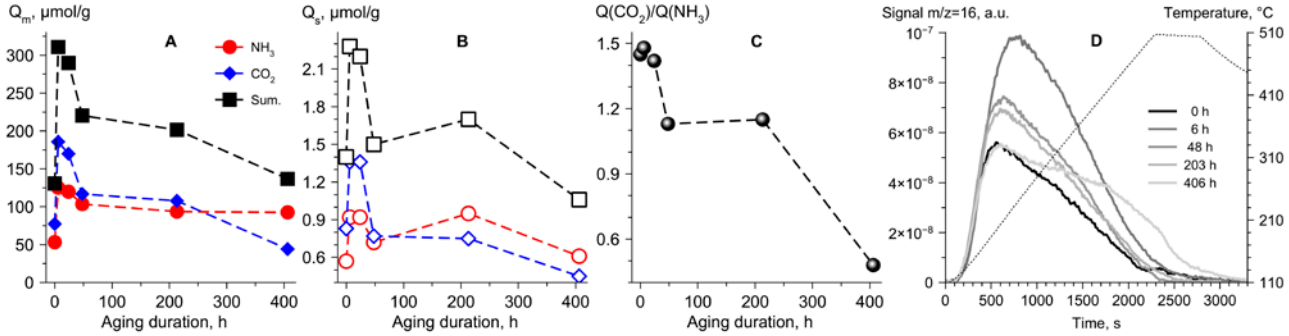

Fig. 8. The dependence of the acidity and basicity of the ZrO_2 surface on the aging duration of $ZrO_2 \cdot nH_2O$

basic properties [42-44]. Further aging led to a decrease in the acidity and basicity of the ZrO_2 surface. What is more, the basicity decreased more than the acidity (Fig. 8B). This effect can be also explained by the participation of terminal OH groups in the attachment of the $ZrO_2 \cdot nH_2O$ PPs and the corresponding decrease in their number relative to the bridging OH groups.

The adsorption strength of the molecular probes, which is directly proportional to the temperature (Fig. 8G), also varied depending on the aging time. An increase in the latter from 0 to 6 h led to a shift in the maximum NH_3desorption peak from 197 to 237 °C; while an increase from 213 to 406 h resulted in an increase in the relative amount of NH_3 desorbed above 400 °C and a decrease in the amount of CO_2 desorbed above 300 °C.

Fourier IR spectroscopy of sorbed pyridine at 150°C (Fig. 9A) and CO_2 at 110°C (Fig. 9B) on ZrO_2 obtained from $ZrO_2 \cdot nH_2O$ with different aging times confirmed the TPD results. An increase in the surface acidity was due to an increase in the number of LAS (1,444 cm^{-1} – 19b, 1,489 cm^{-1} – 19a, 1,574 cm^{-1} – 8b, and 1,604 cm^{-1} – 8a). The number of LAS varied extremely depending on the $ZrO_2 \cdot nH_2O$ aging time, 20 – 78 – 41 μmol/g. Aging also led to the formation of a small number of BAS (1,540 cm^{-1} – 19b and 1,636 cm^{-1} – 8a) (0 – 15 – 10 μmol/g, respectively). CO_2 was sorbed on the surface in the form of mono- (1,680–1,650 cm^{-1}) and bidentate (1,605, 1,470–1,440, and 1,223 cm^{-1}) hydrocarbonates, bidentate carbonates (1,555 and 1,331 cm^{-1}), and bridging (polydentate) carbonates (1,680–1,650 and 1,470–1,440 cm^{-1}). Surface hydrocarbonates were formed with the participation of the ZrO_2 basic (edge) OH-groups, while surface carbonates were formed with the participation of the Zr^{4+}–O^{2-} acid-base pair [42, 45, 46].

3.4. Results and discussion

The described results allow distinguishing two time regions in which different transformations of $ZrO_2 \cdot nH_2O$ occurred during its aging at pH = 10, T = 90 °C:

I. *Region of 0–48 h.* This interval is characterized by the decomposition of $ZrO_2 \cdot nH_2O$ aggregates and agglomerates at all levels: aggregates of nanometer

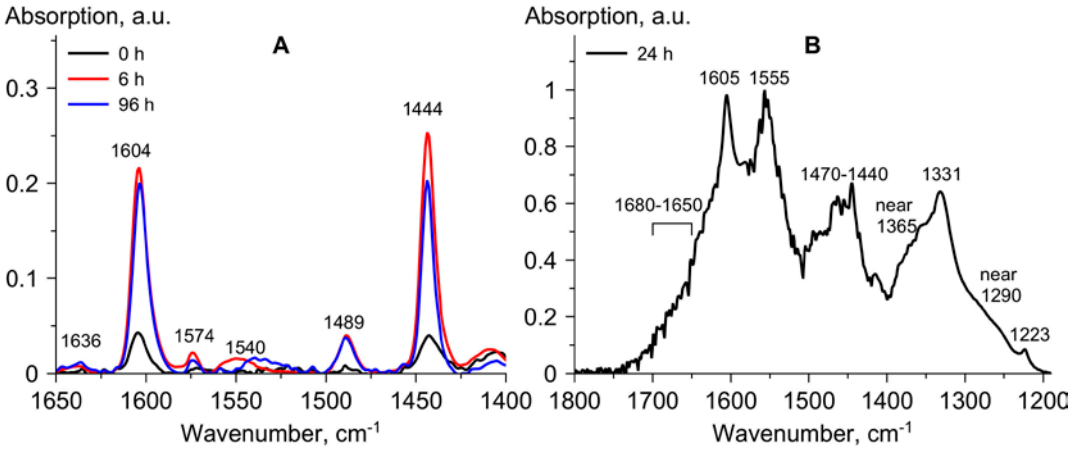

Fig. 9. IR spectra of pyridine (A) and CO_2 sorbed on ZrO_2 obtained by heat treatment at 500 °C $ZrO_2 \cdot nH_2O$ with different aging duration

primary particles (PP), which constituted the walls of micro - and mesopores; and secondary aggregates with the size of hundreds of nm, which constituted large micrometer dense and loose agglomerates. The results of low-temperature N_2 sorption were used to determine the particle size for adsorption, d_{ads}, under the assumption that they can be of different shapes, and to determine the wall thickness of cylindrical pores, 2δ, [9] according to the following formulas:

$$d_{ads} = \frac{A}{\rho \cdot S_{sp}}, \text{ [nm]}, \quad (1)$$

$$2\delta = 2\sqrt{\frac{d_{por}^2}{4} + \frac{d_{por}^2}{4 \cdot \rho \cdot V_\Sigma}} - \frac{d_{por}}{2}, \text{ [nm]}, \quad (2)$$

where A is the particle shape coefficient: 6 – spherical, 4 – rod-like, 2 – plate-like; and $\rho = 4.86$ g/cm³ is the density of X-ray amorphous $ZrO_2 \cdot nH_2O$ [47]. Since $ZrO_2 \cdot nH_2O$ exists in the form of particles rather than a single long cylinder, the thickness of the walls between the pores is 2δ [9]. Assuming that the shape of PPs and their aggregates is plate-like (A = 2), the values of d_{ads} are close to the value of the thickness of pore walls, 2δ (Fig. 10A). This is consistent with the general ideas about the shape of $ZrO_2 \cdot nH_2O$ nanoparticles [48-51] and the estimates based on previous research (Fig. 10B). Therefore, during an aging time of up to 48 h, the PP aggregates in the initial $ZrO_2 \cdot nH_2O$ broke up into their constituent PPs 2 times smaller in size.

Interaction between PPs accompanied by the formation of aggregates occurred through the Zr-O (H)-Zr bridging group, the decomposition of which (Zr-O bond breakage) led to the release of

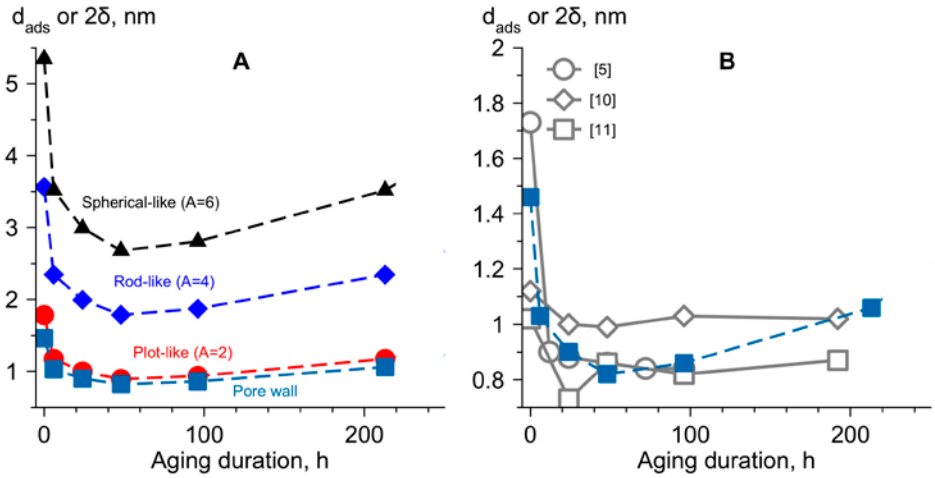

Fig. 10. Changes in the adsorption size of $ZrO_2 \cdot nH_2O$ particles and the thickness of the pore walls depending on the aging duration of $ZrO_2 \cdot nH_2O$ (A) and comparison with the literature data (B)

Zr-OH and an increase in the ratio of terminal OH groups to bridging OH groups. On the other hand, the formation of aggregates can be explained by a combination of hydrogen bonds and dispersion interactions (adhesion) [40]. Then the formation and decomposition of aggregates is of a physical rather than chemical nature. The latter is supported by the fact that the greatest increase in *SSA* was observed during the first 6 hours of aging, during which there was no significant dehydration of $ZrO_2 \cdot nH_2O$ and no change in the ratio between terminal OH groups and bridging OH groups. However, as a result of these processes, some of the additional water molecules and/or OH groups located between the aggregates were removed. This was also confirmed by a 10–12% decrease in the $ZrO_2 \cdot nH_2O$ hydration and decrease in Q_{cr} of aZrO_2 by 16% after 48 h of aging. A change in the type of N_2 sorption isotherms and the hysteresis loop revealed a change in the packing or ordering degree of the PPs and their aggregates: from dense microporous aggregates through loose aggregates of plate-like particles with PP microporosity and mesopores between them, to partially blocked mesopores with narrow mouths or $ZrO_2 \cdot nH_2O$ with an ordered mesoporous grid-like structure.

The presence of PP aggregates in $ZrO_2 \cdot nH_2O$ is a key condition for the formation of *t*-ZrO_2 after heat treatment at 430 and 500 °C, whereas their decomposition to primary particles is a key condition for the formation of *m*-ZrO_2. In terms of factors explaining the stabilization of *t*-ZrO_2 [15, 16], aggregation increased the contribution of interfacial energy, which reached the value necessary for the formation of *t*-ZrO_2. However, the aggregation of $ZrO_2 \cdot nH_2O$ PPs apparently contributed to the formation of nuclei of the necessary local structure, spatial orientation, and ordering [14], while oriented attachment explained the high rate of their formation during thermal crystallization [34]. The decomposition of the $ZrO_2 \cdot nH_2O$ aggregates reduced the role of the initial spatial orientation, local structure and/or ordering of the $ZrO_2 \cdot nH_2O$ PPs and reduced the role of the thermodynamic and kinetic factors of the *t*-ZrO_2 formation. According to the Buyanov-Krivoruchko oriented attachment theory [25], such behavior is characteristic of precipitation consisting of tightly packed (ordered) aggregates. According to this theory, the decomposition of aggregates to PPs is followed by the formation from them of partially crystallized particles, and from those of well-crystallized particles, crystallization centers, which does not lead to a change in the value of *SSA*.

II. *Region of 96–406 h*. In this time region, the primary particles of the X-ray amorphous $ZrO_2 \cdot nH_2O$ formed as a result of the decomposition of aggregates crystallized and formed a mixture of *t*- and *m*-ZrO_2, which was accompanied by intensive dehydration. The ratio of terminal OH groups to bridging OH groups decreased, which indicated the reaction of terminal groups with each other or bridging OH groups resulting in the formation of Zr-O-Zr oxygen bridges (oxolation). This resulted in a decrease in *SSA* and V_Σ, an increase in the diameter and wall thickness of the $ZrO_2 \cdot nH_2O$ and ZrO_2 pores (500 °C), and a denser texture of secondary aggregates and agglomerates.

The fact that as a result of heat treatment at 430 °C, the ratio of crystalline phases was still at about 0.9–1 and was not accompanied by the growth of the crystallites formed at the aging stage indicates the following. The crystallization centers of phases "oriented" the nearest $ZrO_2 \cdot nH_2O$ PPs and the nuclei to get attached and crystallize into secondary crystals exactly with them. The crystallization centers which were formed during 96–213 h of aging also grew by attachment mechanism during further aging for 213–406 h. Apparently, the disordering of the PPs which were formed during 48 h of aging contributed to the possibility of their orientation relative to each other in different spatial configurations, for example, a rod and a "sandwich" [14], with further binding through terminal OH-groups to form nuclei and then crystallization centers. What is more, the probability of such configurations was equal. Apparently, this also required an excess of OH groups in the mother solution and alkaline pH, which contributed to the deformation of nanoparticles [40]. The Buyanov-Krivoruchko oriented attachment theory explains the bimodal distribution of $ZrO_2 \cdot nH_2O$ pore sizes by a higher rate of the formation of secondary crystals during the attachment of nuclei to crystallization centers as compared to the rate of the formation of crystallization centers from nuclei.

4. Conclusions

This paper presents the results of the study of the changes in the phase composition, porosity, and acid-base properties of the $ZrO_2 \cdot nH_2O$ surface and the ZrO_2 nanocrystallites which are formed from it and their dependence on the aging time of $ZrO_2 \cdot nH_2O$ in contact with the mother solution at 90 °C and pH = 10 and in the absence of the influence of impurities (Si^{4+}, Na^+, and K^+). It was established for the first time that in the absence of impurities during aging, the above properties of $ZrO_2 \cdot nH_2O$ and ZrO_2 are extremely dependent on the aging time with an extremum at 24–96 h. It was established that the decomposition of dense aggregates of the primary particles and submicron and micron aggregates and agglomerates of X-ray amorphous $ZrO_2 \cdot nH_2O$ precedes its crystallization into a mixture of *t*- and *m*-ZrO_2 phases, which is described by the Buyanov-Krivoruchko oriented attachment theory. During the decomposition of PP aggregates, $ZrO_2 \cdot nH_2O$ is characterized by the formation of edge OH groups, which participate in the further PP attachment and crystallization. It was assumed that another peculiarity identified during the research, i.e. the ratio of *t*- and *m*-ZrO_2 phases close to 1, which does not change after heat treatment, can be explained by the spatial orientation of PPs during their attachment. The orientation of PPs in dense aggregates of the initial $ZrO_2 \cdot nH_2O$ is a key factor in the formation of nanocrystallites of the *t*-ZrO_2 metastable phase during the heat treatment of $ZrO_2 \cdot nH_2O$.

The revealed features allow expanding the applications of the concepts of the oriented attachment theory to the mild conditions of $ZrO_2 \cdot nH_2O$ aging. From a practical perspective, we determined the aging time of $ZrO_2 \cdot nH_2O$ which makes it possible to achieve the best porosity and acid-base properties of the surface, which are important for the production of ZrO_2-based catalyst supports.

Author contributions

Sh. O. Omarov, research concept, methodology development, text writing, final conclusions, conducting research, review writing, and text editing. M. B. Pakhomov, scientific supervision of research, research concept, and methodology development.

Conflict of interests

The authors declare that they have no known competing financial interests or personal relationships that could have influenced the work reported in this paper.

References

1. Fedorov P. P., Yarotskaya E. G. Zirconium dioxide. Review. *Condensed Matter and Interphases*. 2021;23(2): 169–187. https://doi.org/10.17308/kcmf.2021.23/3427

2. Noskov A. S. Scientific and technical aspects of research and prospects for import substitution in the area of industrial catalysts*. *Vestnik rossiiskoi akademii nauk = Herald of the Russian Academy of Sciences*. 2022;92(10): 940–949. (In Russ). https://doi.org/10.31857/S0869587322100085

3. Gao L., Zhi H., Zhang S., Liu S. Template-free hydrothermal synthesis of octahedron-, diamond-, and plate-like ZrO_2 mono-dispersions. *Nanomaterials*. 2022;12(19): 3405. https://doi.org/10.3390/nano12193405

4. Omarov Sh. O., Pakhomov N. A. Variation of conditions of $ZrO_2 \cdot nH_2O$ precipitation and aging as a method for controlling the phase composition and texture of ZrO_2. *Kataliz v promyshlennosti*. 2020;20(5): 335–43. https://doi.org/10.18412/1816-0387-2020-5-335-343

5. Deshmane V. G., Adewuyi Y. G. Synthesis of thermally stable, high surface area, nanocrystalline mesoporous tetragonal zirconium dioxide (ZrO_2): effects of different process parameters. *Microporous and Mesoporous Materials*. 2012;148(1). https://doi.org/10.1016/j.micromeso.2011.07.012

6. Chuah G. K. An investigation into the preparation of high surface area zirconia. *Catalysis Today*. 1999;49(1–3). https://doi.org/10.1016/s0920-5861(98)00417-9

7. Chuah G. K., Jaenicke S. The preparation of high surface area zirconia - Influence of precipitating agent and digestion. *Applied Catalysis A: General*. 1997;163(1–2). https://doi.org/10.1016/s0926-860x(97)00103-8

8. Chan K. S., Chuah G. K., Jaenicke S. Preparation of stable, high surface area zirconia. *Journal of Materials Science Letters*. 1994;13(21). https://doi.org/10.1007/bf00626515

9. Chuah G. K., Jaenicke S., Pong B. K. The preparation of high-surface-area zirconia: II. Influence of precipitating agent and digestion on the morphology and microstructure of hydrous zirconia. *Journal of Catalysis*. 1998;175(1). https://doi.org/10.1006/jcat.1998.1980

10. Jaenicke S., Chuah G. K., Raju V., Nie Y. T. Structural and morphological control in the preparation of high surface area zirconia. *Catalysis Surveys from Asia*. 2008;12(3). https://doi.org/10.1007/s10563-008-9048-2

11. Chuah G. K., Jaenicke S., Cheong S. A., Chan K. S. The influence of preparation conditions on the surface area of zirconia. *Applied Catalysis A: General*. 1996;145(1–2). https://doi.org/10.1016/0926-860x(96)00152-4

12. Hong E., Baek S. W., Shin M., Suh Y. W., Shin C. H. Effect of aging temperature during refluxing on the textural and surface acidic properties of zirconia catalysts. *Journal of Industrial and Engineering Chemistry*. 2017;54. https://doi.org/10.1016/j.jiec.2017.05.026

13. Sato S., Takahashi R., Sodesawa T., Tanaka S., Oguma K., Ogura K. High-surface-area SiO_2-ZrO_2 prepared by depositing silica on zirconia in aqueous ammonia solution. *Journal of Catalysis*. 2000;196(1). https://doi.org/10.1006/jcat.2000.3027

14. Kuznetsova T. G., Sadykov V. A. Specific features of the defect structure of metastable nanodisperse ceria, zirconia, and related materials. *Kinetics and Catalysis*. 2008;49(6): 840–858. https://doi.org/10.1134/s0023158408060098

15. Shukla S., Seal S. Mechanisms of room temperature metastable tetragonal phase stabilisation in zirconia. *International Materials Reviews*. 2005;50(1). https://doi.org/10.1179/174328005x14267

16. Esposito V., Castelli I. E. Metastability at defective metal oxide interfaces and nanoconfined structures. *Advanced Materials Interfaces*. 2020;7(13). https://doi.org/10.1002/admi.201902090

17. Strekalovsky V. N., Polezhaev Yu. M., Palyguev S. F. *Oxides with impurity disordering: composition, structure, and phase transformations*. Moscow: Nauka Publ.; 1987. 160 p. (In Russ).

18. Brown P. *Chemical thermodynamics of zirconium*. Amsterdam: Elsevier; 2005. 542 p.

19. Sasaki T., Kobayashi T., Takagi I., Moriyama H. Hydrolysis constant and coordination geometry of zirconium(IV). *Journal of Nuclear Science and Technology*. 2008;45(8): 735–739. https://doi.org/10.1080/18811248.2008.9711474

20. Kobayashi T., Bach D., Altmaier M., Sasaki T., Moriyama H. Effect of temperature on the solubility and solid phase stability of zirconium hydroxide. *Radiochimica Acta*. 2013;101(10). https://doi.org/10.1524/ract.2013.2074

21. Denkewicz R. P., TenHuisen K. S., Adair J. H. Hydrothermal crystallization kinetics of m-ZrO_2 and *t*-ZrO_2. *Journal of Materials Research*. 1990;5(11). https://doi.org/10.1557/jmr.1990.2698

22. Ivanov V. K., Fedorov P. P., Baranchikov A. Y., Osiko V. V. Oriented attachment of particles: 100 years of investigations of non-classical crystal growth. *Russian Chemical Reviews*. 2014;83(12): 1204–1222. https://doi.org/10.1070/rcr4453

23. Pathiraja G., Obare S., Rathnayake H. Oriented attachment crystal growth dynamics of anisotropic one-dimensional metal/metal oxide nanostructures: mechanism, evidence, and challenges. In: *Crystal Growth and Chirality - Technologies and Applications*. 2023. https://doi.org/10.5772/intechopen.107463

24. He W., Wen K., Niu Y. Introduction to oriented-attachment growth mechanism. In: *Springer Briefs in Energy*. Switzerland: Springer; 2018. 84 p. https://doi.org/10.1007/978-3-319-72432-4_1

25. Buyanov R. A., Krivoruchko O. P. Development of the theory of crystallization of low-soluble metal hydroxides and scientific foundations for the preparation of catalysts from substances of this class*. *Kinetics and Catalysis*. 1976;17(3): 765–75. (In Russ). Available at: https://www.elibrary.ru/item.asp?id=22694458

26. Zi W., Hu Z., Jiang X., ... Liu, F. Morphology regulation of zeolite MWW via classical/nonclassical crystallization pathways. *Molecules*. 2023;29(1): 170. https://doi.org/10.3390/molecules29010170

27. Xia Y., Shi J., Sun Q., ... Chen J.-F. Controllable synthesis and evolution mechanism of monodispersed Sub-10 nm ZrO_2 nanocrystals. *Chemical Engineering Journal*. 2020;394. 124843. https://doi.org/10.1016/j.cej.2020.124843

28. Xu X., Wang X. Fine tuning of the sizes and phases of ZrO_2 nanocrystals. *Nano Research*. 2009;2(11). https://doi.org/10.1007/s12274-009-9092-x

29. Pokratath R., Lermusiaux L., Checchia S., ... De Roo J. An amorphous phase precedes crystallization: unraveling the colloidal synthesis of zirconium oxide nanocrystals. *ACS Nano*. 2023;17(9): 8796–8806. https://doi.org/10.1021/acsnano.3c02149

30. Stolzenburg P., Freytag A., Bigall N. C., Garnweitner G. Fractal growth of ZrO_2 nanoparticles induced by synthesis conditions. *CrystEngComm*. 2016;18(43). https://doi.org/10.1039/c6ce01916a

31. Yan H., Di J., Li J., Liu Z., Liu J., Ding X. Synthesis of zirconia micro-nanoflakes with highly exposed (001) facets and their crystal growth. *Crystals*. 2021;11(8). https://doi.org/10.3390/cryst11080871

32. Qin W., Zhu L. Anisotropic morphology, formation mechanisms, and fluorescence properties of zirconia nanocrystals. *Scientific Reports*. 2020;10(1). https://doi.org/10.1038/s41598-020-70570-5

33. Ribeiro C., Vila C., De Matos J. M. E., Bettini J., Longo E., Leite E. R. Role of the oriented attachment mechanism in the phase transformation of oxide nanocrystals. *Chemistry – A European Journal*. 2007;13(20). https://doi.org/10.1002/chem.200700034

34. Almyasheva O. V. *Formation of oxide nanocrystals and nanocomposites in hydrothermal conditions and the structure and properties of materials based on them**. Dr. Sci. (Chem.) diss. Saint-Petersburg: 2017. 363 c. Available at: https://www.dissercat.com/content/formirovanie-oksidnykh-nanokristallov-i-nanokompozitov-v-gidrotermalnykh-usloviyakh-stroenie (In Russ).

35. Chuah G. K., Jaenicke S., Xu T. H. Acidity of high-surface-area zirconia prepared from different precipitants. *Surface and Interface Analysis*. 1999;28(1): 131–134. https://doi.org/10.1002/(sici)1096-9918(199908)28:1<131::aid-sia634>3.0.co;2-5

36. Toraya H., Yoshimura M., Somiya S. Calibration curve for quantitative analysis of the monoclinic-tetragonal ZrO_2 system by X-ray diffraction. *Journal of American Ceramic Society*. 1984;67: C119–121. https://doi.org/10.1111/j.1151-2916.1984.tb19715.x

37. Emeis C. A. Determination of integrated molar extinction coefficients for infrared absorption bands of pyridine adsorbed on solid acid catalysts. *Journal of Catalysis*. 1993;141(2): 347–354. https://doi.org/10.1006/jcat.1993.1145

38. King G., Soliz J. R., Gordon W. O. Local structure of $Zr(OH)_4$ and the effect of calcination temperature from X-ray pair distribution function Analysis. *Inorganic Chemistry*. 2018;57(5). https://doi.org/10.1021/acs.inorgchem.7b03137

39. Mogilevsky G., Karwacki C. J., Peterson G. W., Wagner G.W . Surface hydroxyl concentration on $Zr(OH)_4$ quantified by 1H MAS NMR. *Chemical Physics Letters*. 2011;511(4–6): 384–388. https://doi.org/10.1016/j.cplett.2011.06.072

40. Iordanov I. O., Bermudez V. M., Knox C. K. Computational modeling of the structure and properties of

$Zr(OH)_4$. *Journal of Physical Chemistry C*. 2018;122(10). https://doi.org/10.1021/acs.jpcc.7b11107

41. Li J., Chen J., Song W., Liu J., Shen W. Influence of zirconia crystal phase on the catalytic performance of Au/ZrO_2 catalysts for low-temperature water gas shift reaction. *Applied Catalysis A: General*. 2008;334(1–2). https://doi.org/10.1016/j.apcata.2007.10.020

42. Wan E., Travert A., Quignard F., Tichit D., Tanchoux N., Petitjean H. Modulating properties of pure ZrO_2 for structure–activity relationships in acid-base catalysis: contribution of the alginate preparation route. *ChemCatChem*. 2017;9(12): 2358–2365. https://doi.org/10.1002/cctc.201700171

43. Ouyang F., Nakayama A., Tabada K., Suzuki E. Infrared study of a novel acid–base site on ZrO_2 by adsorbed probe molecules. I. pyridine, carbon dioxide, and formic acid adsorption. *The Journal of Physical Chemistry B*. 2000;104(9): 2012–2018. https://doi.org/10.1021/jp992970i

44. Ma Z. Y., Yang C., Wei W., Li W. H., Sun Y. H. Surface properties and CO adsorption on zirconia polymorphs. *Journal of Molecular Catalysis A: Chemical*. 2005;227(1–2). https://doi.org/10.1016/j.molcata.2004.10.017

45. Ouyang H., Li C., Li K., Li H., Zhang Y. Effect of pH on crystallization of nanocrystalline zirconia in a microwave-hydrothermal process. *Journal Wuhan University of Technology, Materials Science Edition*. 2016;31(1). https://doi.org/10.1007/s11595-016-1332-9

46. Köck E. M., Kogler M., Götsch T., … Penner S. Surface chemistry of pure tetragonal ZrO_2 and gas-phase dependence of the tetragonal-to-monoclinic ZrO_2 transformation. *Dalton Transactions*. 2017;46(14): 4554–4570. https://doi.org/10.1039/c6dt04847a

47. Ceresoli D., Vanderbilt D. Structural and dielectric properties of amorphous ZrO_2 and HfO_2. *Physical Review B*. 2006;74(12): 125108. https://doi.org/10.1103/physrevb.74.125108

48. Livage J., Doi K., Mazieres C. Nature and thermal evolution of amorphous hvdrated zirconium oxide. *Journal of the American Ceramic Society*. 1968;51(6): 349–353. https://doi.org/10.1111/j.1151-2916.1968.tb15952.x

49. Azarova L. A., Kopitsa G. P., Yashina E. G., Garamus V. M., Grigoriev S. V. The model of fractal particle of hydrated zirconium dioxide based on small-angle neutron scattering data. *Journal of Surface Investigation: X-Ray, Synchrotron and Neutron Techniques*. 2019;(10): 23–29. (In Russ, abstract in Eng.). https://doi.org/10.1134/S0207352819100044

50. Ivanov V. K., Kopitsa G. P., Baranchikov A. E., Grigoriev S. V., Garamus V. M. Regularities of changes in composition and fractal structure of hydrated zirconium dioxide xerogels during thermal annealing*. *Russian Journal of Inorganic Chemistry*. 2010;55(2): 190–196. (In Russ). Available at: https://www.elibrary.ru/item.asp?id=13725937

51. Tiseanu C., Parvulescu V. I., Sanchez-Dominguez M., Boutonnet M. Spectrally and temporarily resolved luminescence study of short-range order in nanostructured amorphous ZrO_2. *Journal of Applied Physics*. 2011;110(10). https://doi.org/10.1063/1.3662117

** Translated by author of the article*

Information about the authors

Shamil O. Omarov, postgraduate student, Research Fellow, Ioffe Institute (Saint-Petersburg, Russian Federation).
https://orcid.org/0000-0002-6862-128X
somarov@mail.ioffe.ru

Nikolay A. Pakhomov, Cand. Sci (Chem.), Research Fellow, St. Petersburg State Technological Institute (Technical University) (Saint-Petersburg, Russian Federation).
https://orcid.org/0009-0001-8414-2561
npakhomov@technolog.edu.ru

Received 05.08.2024; approved after reviewing 20.08.2024; accepted for publication 16.09.2024; published online 25.12.2024.

Translated by Irina Charychanskaya